IRis

Northeastern University

Physics Faculty Publications

Department of Physics

May 08, 2007

Nodeless d-wave superconducting pairing due to residual antiferromagnetism in underdoped Pr2-xCexCuO4-δ

Tanmoy Das
Northeastern University

R. S. Markiewicz
Northeastern University

A. Bansil
Northeastern University

Recommended Citation

Das, Tanmoy; Markiewicz, R. S.; and Bansil, A., "Nodeless d-wave superconducting pairing due to residual antiferromagnetism in underdoped Pr2-xCexCuO4-δ" (2007). *Physics Faculty Publications.* Paper 403.

This work is available open access, hosted by Northeastern University.

Nodeless d-Wave Superconducting Pairing due to Residual Antiferromagnetism in Underdoped $Pr_{2-x}Ce_xCuO_{4-\delta}$

Tanmoy Das, R. S. Markiewicz, and A. Bansil
Physics Department, Northeastern University, Boston, Massachusetts 02115, USA
(Received 6 November 2006; published 8 May 2007)

We investigate the doping dependence of the penetration depth versus temperature in electron-doped $Pr_{2-x}Ce_xCuO_{4-\delta}$ using a model which assumes the uniform coexistence of (mean-field) antiferromagnetism and superconductivity. Despite the presence of a $d_{x^2-y^2}$ pairing gap in the underlying spectrum, we find nodeless behavior of the low-T penetration depth in the underdoped case, in accord with experimental results. As doping increases, a linear-in-T behavior of the penetration depth, characteristic of d-wave pairing, emerges as the lower magnetic band crosses the Fermi level and creates a nodal Fermi surface pocket.

DOI: 10.1103/PhysRevLett.98.197004 PACS numbers: 74.20.Rp, 74.20.Mn, 74.25.Dw, 74.25.Nf

An understanding of the symmetry of the order parameter and its evolution with hole and electron doping is a key to unraveling the mechanism of high-T_c superconductivity in cuprates. Many experimental and theoretical studies of these fascinating materials demonstrate the presence of antiferromagnetic (AFM) order in underdoping for both hole [1] and electron doping [2–4]. With hole doping, the route followed by the AFM phase as it develops into the superconducting (SC) phase involves the intervention of nanoscale phase separations related to stripe or pseudogap physics [1]. The behavior with electron doping, on the other hand, seems to be simpler in that the doped phase appears to be a uniform AFM metal, possibly evolving into a phase with coexisting AFM and SC orders [2–4].

For the hole doped cuprates it is generally believed that d-wave pairing survives up to the edge of antiferromagnetism [1,5,6], but the doping dependence of the pairing symmetry with electron doping remains a matter of debate. This symmetry has been studied by low-T penetration depth (PD) measurements [7–12], point contact spectroscopy [13,14], tunneling [15], and other phase sensitive probes [16], in a variety of electron-doped cuprates, including $Nd_{2-x}Ce_xCuO_{4-\delta}$ (NCCO) [7–10,16], $La_{2-x}Ce_xCuO_{4-\delta}$ (LCCO) [11,15], and $Pr_{2-x}Ce_xCuO_{4-\delta}$ (PCCO) [11–14]. The results have been contradictory, with some early measurements [7–10] finding evidence for s-wave pairing, while other experiments suggest a transition from d-wave in underdoping to either s-wave [11,13] or $(d + is)$-wave character [14] in the optimally and overdoped cases. Yet other experiments [12,16] report only d-wave pairing, with the situation further complicated by the presence of nonmonotonic SC-gap variations observed in NCCO [17] and $Pr_{1-x}LaCe_xCuO_{4-\delta}$ (PLCCO) [2].

A recent study approximated the AFM background by treating the resulting partially gapped Fermi surface (FS) in a two band model [18]. To understand the interplay between AFM and SC orders and the role of AFM order in modifying the pairing [19,20], in this Letter we directly evaluate the PD in a model with coexisting AFM and SC order. We assume a SC gap of d-wave pairing with a combination of first and third harmonics, which is necessary to incorporate nonmonotonic gap variations [2,17]. We find that even in the presence of a d-wave pairing gap, the PD varies exponentially at low T for most dopings—a behavior characteristic of a nodeless SC gap, as antiferromagnetism suppresses the spectral weight from the nodal point. In the overdoped case ($x = 0.152$), the PD shows a linear-in-T behavior as the hole pocket forms in the nodal region. Our analysis indicates that with increasing electron doping the position of the maximum leading edge gap on the FS moves away from the antinodal direction and that the nonmonotonic nature of the gap becomes stronger.

Our treatment of the in-plane PD is based on the Hamiltonian

$$H = H_{\text{pair}} + H_{\text{int}}, \tag{1}$$

where H_{pair} describes the physics of coexisting AFM and SC orders. We take H_{pair} to be a one-band, tight-binding Hubbard Hamiltonian along the lines of Ref. [4] in which the SC gap is of d-wave pairing with a combination of first and third harmonics. The tight-binding parameters are assumed to be same as for NCCO [3]. The external perturbation is given by the electromagnetic interaction,

$$H_{\text{int}} = -\left(\frac{e}{c}\right)\vec{A}\cdot\left[\sum_{\vec{k},\sigma}\vec{v}_{\vec{k}}c^{\dagger}_{\vec{k},\sigma}c_{\vec{k},\sigma}\right], \tag{2}$$

where $c^{\dagger}_{\vec{k},\sigma}$ ($c_{\vec{k},\sigma}$) is the electronic creation (destruction) operator with momentum $\vec{k}$, charge e and spin σ, and c is speed of light. $\vec{A}$ is the Fourier component of the vector potential in momentum space. $\vec{v}_{\vec{k}} = \partial\xi_{\vec{k}}/(\hbar\partial\vec{k})$ is the band velocity for the noninteracting band $\xi_{\vec{k}}$ [3].

The PD is obtained by evaluating the induced current parallel to the vector potential, which is proportional to the inverse square of the in-plane PD [21]. We have generalized the pure BCS result to the mixed AFM-SC case and find [22]

 © 2007 The American Physical Society

$$\lambda_{ij}^{-2}(T) = \frac{4\pi e^2}{c^2 a^2 d} \sum_{\nu=\pm} \sum_{\vec{k}}{}' \left\{ \left(\frac{1}{m_{\vec{k}ij}^{\nu}} \right) \left[1 - \frac{\xi_{\vec{k}}^{+} + \nu E_{0\vec{k}}}{E_{\vec{k}}^{\nu}} \times \tanh(\beta E_{\vec{k}}^{\nu}/2) \right] - \frac{\beta}{2} v_{\vec{k}i}^{\nu} v_{\vec{k}j}^{\nu} \mathrm{sech}^2(\beta E_{\vec{k}}^{\nu}/2) \right\}. \quad (3)$$

Here, a is the in-plane and d the out-of-plane lattice constant of PCCO and $\beta = 1/k_B T$. The prime on the $\vec{k}$ summation means that the sum is restricted to wave vectors in the magnetic zone. The magnetic field is assumed to lie perpendicular to the CuO_2 plane. For a tetragonal lattice λ_{ij} is diagonal, with $\lambda_{aa} = \lambda_{bb} = \lambda$ within the CuO_2 plane. Interestingly, Eq. (3) displays a form similar to that for a pure d-wave SC [23,24], excepting two modifications. First, the FS has components $\nu = \pm$ associated with the upper magnetic band (UMB) and the lower magnetic band (LMB), respectively:

$$(E_{\vec{k}}^{\nu})^2 = (\xi_{\vec{k}}^{+} + \nu E_{0\vec{k}})^2 + \Delta_{\vec{k}}^2, \quad (4)$$

where $E_{0\vec{k}} = \sqrt{(\xi_{\vec{k}}^{-})^2 + (U_Q S)^2}$ and $\xi_{\vec{k}}^{\pm} = (\xi_{\vec{k}} \pm \xi_{\vec{k}+\vec{Q}})/2$. $\Delta_{\vec{k}}$ is the SC gap and $U_Q S$ the AFM gap in terms of the AFM repulsion U_Q and the commensurate magnetization S at the nesting vector $Q = (\pi, \pi)$. Second, the band masses $m_{\vec{k}ij}^{\nu}$ and quasiparticle velocities $\vec{v}_{\vec{k}}^{\nu}$ have magnetic correlation corrections: $1/m_{\vec{k}ij}^{\nu} = \partial^2(\xi_{\vec{k}}^{+} + \nu E_{0\vec{k}})/(\hbar^2 \partial k_i \partial k_j)$, $\vec{v}_{\vec{k}}^{\nu} = \partial(\xi_{\vec{k}}^{+} + \nu E_{0\vec{k}})/(\hbar \partial \vec{k})$.

We obtain the AFM and SC gaps self-consistently as a function of T for a series of doping levels over the range $x = 0.115$–0.152, using doping dependent interaction parameters [4], before proceeding with the PD calculation from Eq. (3). The effective AFM interaction given by U_Q is taken from our earlier work on NCCO [3] and decreases from a value of $3.33t$ at $x = 0.115$ to $3.1t$ at $x = 0.152$; the resulting self-consistent magnetization S decreases linearly from 0.2 to 0.13 over this doping range, in agreement with earlier results [3], despite the presence of the SC order.

The two terms on the right-hand side of Eq. (3) correspond to the conventional diamagnetic (first term) and paramagnetic [25] (second term) currents of electrons. In a London picture, $\lambda^{-2}(T)$ is proportional to the SC electron density n_s and hence vanishes as $T \to T_c$, while at $T = 0$ all the electrons are superconducting. Here we find a similar result, but only the electrons in the AFM pockets condense. Similarly, as $T \to 0$, the linear-in-T PD found in overdoped samples reveals the presence of gap nodes, where normal quasiparticles persist to zero energy.

Figure 1 compares the theoretical and experimental values of the inverse square of the PD in PCCO [26] over the doping range $x = 0.115$–0.152. The results are normalized to the computed $T = 0$ value for the c-axis lattice constant $d = 12.2$ Å [27] in order to highlight T dependencies. The overall agreement is quite good, allowing us to adduce the doping dependence of the AFM and SC properties as discussed below. A discrepancy is found at the lowest and highest dopings, where the PD shows a tail extending beyond T_c, possibly associated with sample inhomogeneities [28].

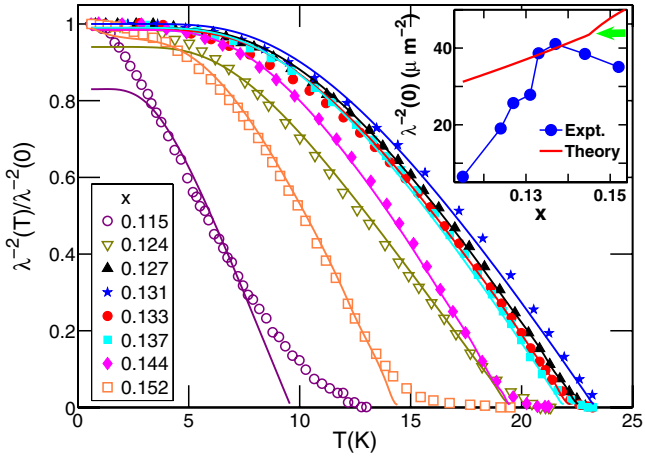

FIG. 1 (color online). Various colored lines give computed $\lambda^{-2}(T)/\lambda^{-2}(0)$ as a function of T for different dopings x; the corresponding experimental data for PCCO [26] are shown by symbols of the same color (see legend). Inset: computed (red line) and experimental (blue dots) values of $\lambda^{-2}(0)$ as a function of doping. Green arrow points to the *kink* associated with the opening of the nodal pocket in the theory curve.

Turning to the inset in Fig. 1, note first that the theoretical values (red line) of $\lambda^{-2}(0) \propto n_s(0)$, do not involve any further fitting parameters beyond those used in fitting the T dependence of λ. Around optimal doping, theory and experiment are seen to be in accord indicating that the theory correctly predicts the value of $n_s(0)$, although striking deviations are seen away from optimal doping. Insight into this behavior is obtained by observing that as $T \to 0$, all the electrons on the FS condense so that $n_s(0)$ is proportional to the area of the FS pockets. For this reason, the computed $n_s(0)$ decreases linearly with underdoping and undergoes a change in slope (marked by the green arrow) as the $(\pi/2, \pi/2)$ pocket crosses the Fermi level in overdoping. In sharp contrast, the experimental points (blue dots) present a peak around optimal doping and a loss of carriers away from optimal doping, indicative of "bad metal" physics where the SC transition is dominated by thermal phase fluctuations [29,30]. These results suggest that on the underdoped side AFM fluctuations are more deleterious than expected from the mean-field BCS model underlying our computations. The reappearance of bad metal behavior on overdoping is puzzling and its origin is unclear—it may be related to increasing doping-induced disorder.

We discuss the doping and T dependencies of the preceding theoretical PD results with reference to Figs. 2–4. In Fig. 2(a), we emphasize that the contribution of the UMB is nodeless since the PD is dominated by energies near the Fermi level and the UMB pocket is far from the nodal region. An exponential form, $1 - C\exp(-\beta D)$, is

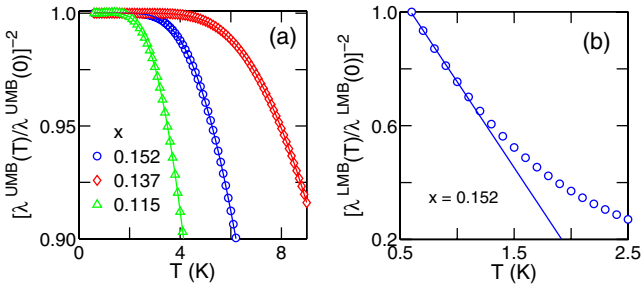

FIG. 2 (color online). (a) UMB contribution to the theoretical PD at three different dopings. Solid lines give the corresponding exponential fits of form $[1 - C\exp(-\beta D)]$ at low T. (b) LMB contribution at $x = 0.152$ (○) and the related linear fit, $(1 - aT)$, at low T (blue line).

seen to produce an excellent fit in the low-T region in Fig. 2(a). The values of the SC gap D in Fig. 3(a) so obtained for the UMB (blue dots) are quite close to the SC gap (red open squares) at the electron pocket tip, marked by yellow diamonds on the FS plots of Figs. 4(b)–4(d). The value of C is ≈ 4.4, essentially independent of doping. Only at the highest doping $x = 0.152$ do we find a significant linear-in-T (d-wave) contribution to the PD as shown in Fig. 2(b), which coincides with the appearance of the hole pocket near $(\pi/2, \pi/2)$ at high dopings as the LMB crosses the Fermi level [see Fig. 4(d)]. A linear equation of the form, $1 - aT$, fits the LMB contribution very well up to $T = 1.5$ K as shown by blue line in Fig. 2(b) [31]. We do not find a second regime of linear-in-T PD in the strongly underdoped regime [19].

Figure 3 examines the doping dependence of the SC-gap parameters. The domelike shape as a function of doping of the gap D in Fig. 3(a) is reflected in the behaviors of the first and third harmonics of the pairing gap in Fig. 3(b) as well. Figure 3(c) delineates the doping dependence of the first and third harmonics of the pairing interaction, which display a maximum near $x \approx 0.13$ where T_c is optimal. The doping dependence of the SC-gap parameters Δ_1 and Δ_3 is compared with various experimental results in Figs. 3(b) and 3(d). Some disagreement with Raman experiments on NCCO (green filled squares) and PCCO (green open squares) [32] is due to sample variations, reflected in T_c variations, while the ratio $2\Delta_1/k_BT_c$ is

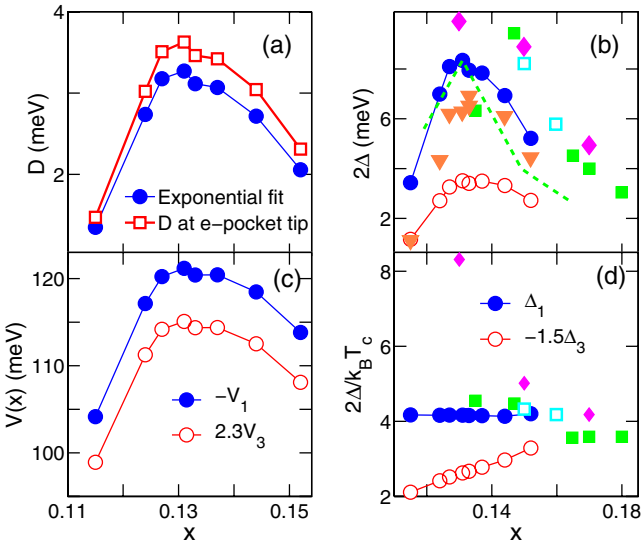

FIG. 3 (color online). (a) SC gap D as a function of doping obtained from exponential fits similar to those in Fig. 2(a) at low T (blue dots), and the values of the SC gap (red open squares) at the tip of the electron pockets, shown in Fig. 4(b)–4(d) (yellow diamonds). (b) Self-consistent first harmonic $2\Delta_1$ (blue dots) and third harmonic $-4\Delta_3$ (red open circles) of the SC gap are compared with several experimental results for NCCO and PCCO: Raman scattering in B_{2g} channel from NCCO [PCCO] [32], green filled [green open] squares; tunneling data on NCCO [13,14], magenta diamonds; two band model computations [18], orange triangles. Green dashed line shows the scaled Raman B_{2g} channel gap for NCCO. (c) SC interaction potentials as a function of doping: absolute value of the d-wave first harmonic $-V_1$ (blue dots) and the third harmonics $2.3V_3$ (red circles). (d) $2\Delta/k_BT_c$ for Δ_1 and $-1.5\Delta_3$ for the first and third harmonic SC gaps are compared to the experimental results. Various symbols have the same meanings as in (b).

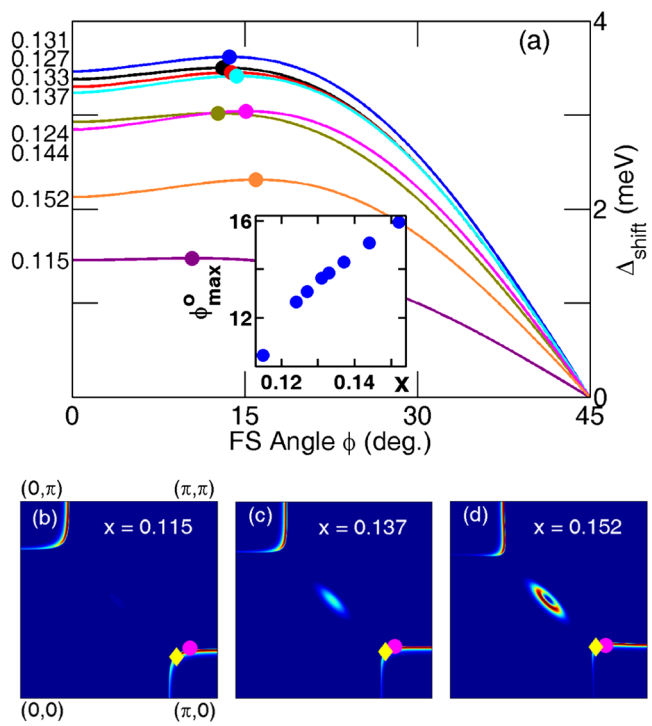

FIG. 4 (color online). (a) Variation in the leading edge gap (LEG), $\Delta_{\rm shift}$, over the FS in terms of the FS angle ϕ, where ϕ increases from zero along the antinodal direction to 45° along the nodal direction. Solid dots mark positions of the LEG maximum, $\phi_{\rm max}$, which is seen in the inset to increase nearly linearly with doping. (b)–(d) FS is calculated for three different dopings x. Red color denotes maximum spectral weight and blue color zero intensity. Red dots give the position of the maximum LEG gap on the FS considered in (a). Yellow diamonds mark the tips of the UMB electron pockets, at which the SC gaps in Fig. 2(a) were calculated.

essentially constant and agrees well with experiment. If we scale the experimental gap to fit the calculated maximum at optimal doping, we can reproduce the domelike behavior of the SC gap as shown by the green dashed line in Fig. 3(b) for NCCO. The tunneling data (magenta diamonds) [13,14] do not show a maximum, because tunneling is sensitive to the *total gap* obtained by combining AFM and SC gaps, and this combined gap in our computations does not have a maximum near optimal doping. Similarly, the larger gap seen by Raman [32] in under and optimally doped samples can be understood since the B_{2g} channel measures the total spectral gap near the $(\pi, 0)$ point [33], and hence is strongly coupled to the AFM order.

Figure 3(d) shows that the ratio $2\Delta_1/k_BT_c$ possesses a nearly constant value of 4.1 close to the BCS value for a d-wave gap. In contrast, for fixed ratio of V_1/V_3 [34], the third harmonic ratio $-2\Delta_3/k_BT_c$ increases linearly with doping. This is the reason that the position of the maximum of the leading edge gap (LEG) $\Delta_{\rm shift}$ on the FS, given by the FS angle $\phi_{\rm max}$ in Fig. 4(a), moves away from the antinodal point with doping; interestingly, the hot spots also move away with doping from the antinodal direction, but their shift is much smaller. We find that the ratio of the maximum value of $\Delta_{\rm shift}$ to its value along the antinodal direction increases with doping, indicating that the nonmonotonic nature of d-wave pairing symmetry becomes more pronounced as one goes from under to overdoping in the electron-doped cuprates.

The evolution of the $(\pi/2, \pi/2)$-centered nodal hole pocket is seen in Figs. 4(b)–4(d). The absence of nodal pockets in the underdoped regime [see Fig. 4(b)] is responsible for the nodeless behavior of the SC gap. At optimal doping $x = 0.137$, the hole pocket is still $\sim$25 meV below E_F, but can be seen in Fig. 4(c) due to the finite energy resolution. The nodal pocket is fully formed in the overdoped case of Fig. 4(d) which is related to the striking d-wave behavior of PD in Fig. 2(b) as well as the kink in $n_s(0)$ in Fig. 1 inset.

In conclusion, we have shown that the linear-in-T variation of λ^{-2} in electron-doped cuprates is related to the appearance of the $(\pi/2, \pi/2)$-nodal hole pocket on the FS, which occurs in the overdoped regime. In underdoping, where the FS only consists of the $(\pi, 0)$-centered electron pockets, λ^{-2} varies in a nodeless manner, even though the pairing interaction is of d-wave symmetry, because the electron pocket lies far from the nodal region. Our analysis indicates that the SC electron density $[n_s(0)]$ is suppressed in a non-BCS fashion as one goes away from optimal doping to either under or overdoping. Interestingly, we find that the SC interaction (V_1 and V_3) also peaks at optimal doping.

This work is supported by the US DOE Contracts No. DE-FG02-07ER46352 and No. DE-AC03-76SF00098 and benefited from the allocation of supercomputer time at NERSC and Northeastern University's Advanced Scientific Computation Center (ASCC).

[1] A. Hosseini *et al.*, Phys. Rev. Lett. **93**, 107003 (2004), and references therein.
[2] H. Matsui *et al.*, Phys. Rev. Lett. **95**, 017003 (2005).
[3] C. Kusko *et al.*, Phys. Rev. B **66**, 140513(R) (2002).
[4] Tanmoy Das *et al.*, Phys. Rev. B **74**, 020506(R) (2006).
[5] Y. Dagan and G. Deutscher, Phys. Rev. Lett. **87**, 177004 (2001).
[6] C. C. Tsuei *et al.*, Phys. Rev. Lett. **93**, 187004 (2004).
[7] D. H. Wu *et al.*, Phys. Rev. Lett. **70**, 85 (1993); S. M. Anlage *et al.*, Phys. Rev. B **50**, 523 (1994).
[8] A. Andreone *et al.*, Phys. Rev. B **49**, 6392 (1994).
[9] C. W. Schneider *et al.*, Physica (Amsterdam) **233C**, 77 (1994).
[10] L. Alff *et al.*, Eur. Phys. J. B **5**, 423 (1998); S. Kashiwaya *et al.*, Phys. Rev. B **57**, 8680 (1998).
[11] J. A. Skinta *et al.*, Phys. Rev. Lett. **88**, 207005 (2002).
[12] A. Snezhko *et al.*, Phys. Rev. Lett. **92**, 157005 (2004).
[13] A. Biswas *et al.*, Phys. Rev. Lett. **88**, 207004 (2002).
[14] M. M. Qazilbash *et al.*, Phys. Rev. B **68**, 024502 (2003).
[15] B. Chesca *et al.*, Phys. Rev. B **71**, 104504 (2005).
[16] Ariando *et al.*, Phys. Rev. Lett. **94**, 167001 (2005).
[17] G. Blumberg *et al.*, Phys. Rev. Lett. **88**, 107002 (2002).
[18] H. G. Luo and T. Xiang, Phys. Rev. Lett. **94**, 027001 (2005).
[19] K.-K. Voo and W. C. Wu, Physica (Amsterdam) **417C**, 103 (2005).
[20] Q. Yuan *et al.*, Phys. Rev. B **74**, 214503 (2006).
[21] M. Tinkham, *Introduction to Superconductivity* (McGraw-Hill, New York, 1996), 2nd ed.
[22] A similar result is found in a d-density wave SC, Q. H. Wang *et al.*, Phys. Rev. Lett. **87**, 077004 (2001).
[23] S. Misawa, Phys. Rev. B **51**, 11 791 (1995); Phys. Rev. B **49**, 6305 (1994).
[24] D. E. Sheehy *et al.*, Phys. Rev. B **70**, 054510 (2004).
[25] The effect of Pr^{3+} paramagnetism on the PD is neglected. [J. R. Cooper, Phys. Rev. B **54**, R3753 (1996)].
[26] M.-S. Kim *et al.*, Phys. Rev. Lett. **91**, 087001 (2003).
[27] J. T. Markert *et al.*, Phys. Rev. Lett. **64**, 80 (1990).
[28] The two band model [18] finds a different interpretation for these tails, which we are unable to reproduce.
[29] V. J. Emery and S. A. Kivelson, Nature (London) **374**, 434 (1995); E. W. Carlson *et al.*, Phys. Rev. Lett. **83**, 612 (1999).
[30] A very small n_s may explain the deviations in the T dependence of PD for the lowest doped sample.
[31] Disorder-induced T^2 contribution [P. J. Hirschfeld and N. Goldenfeld, Phys. Rev. B **48**, 4219(R) (1993)] could improve the fit for PD in the $x = 0.152$ sample but not in the lower doping (exponential) regime.
[32] M. M. Qazilbash *et al.*, Phys. Rev. B **72**, 214510 (2005).
[33] C. S. Liu *et al.*, Phys. Rev. B **73**, 174517 (2006).
[34] T_c for each doping is adjusted to produce the best agreement with the experimental PD data and, in order to reduce the number of parameters, the ratio between the SC interactions V_1 and V_3 has been kept fixed at a value of 2.4 for all dopings.